Journal of Innovative Optical Health Sciences
Vol. 5, No. 3 (2012) 1250016 (6 pages)

DOI: 10.1142/S1793545812500162

SUPPRESSION OF SIDELOBES IN SINGLE-PHOTON 4PI CONFOCAL MICROSCOPY BY FÖRSTER RESONANT ENERGY TRANSFER

JIANFANG CHEN
Shanghai Institute of Optics and Fine Mechanics
Chinese Academy of Sciences, No. 390, Qinghe Road, Jiading
P. O. Box 800-211, Shanghai 201800, P. R. China
cjianfang@hotmail.com

YA CHENG
State Key Laboratory of High Field Laser Physics
Shanghai Institute of Optics and Fine Mechanics
Chinese Academy of Sciences, No. 390, Qinghe Road, Jiading
P. O. Box 800-211, Shanghai 201800, P. R. China
ya.cheng@siom.ac.cn

Accepted 11 June 2012
Published 15 August 2012

Recently, we theoretically demonstrate that utilization of silica nanobeads co-doped with Cy3 and Cy5 molecules instead of single dye molecules as fluorescent labels can enable optical resolutions far beyond the diffraction-limit. Here, we show that by combining the 4Pi microscopy and the novel fluorescent label, it is possible to completely suppress the sidelobes in 4Pi focal spot and significantly enhance the optical resolution in the axial direction.

Keywords: Fluorescent dye; 4Pi microscopy; far-field imaging; super-resolution; confocal.

1. Introduction

Optical microscopy has long been an indispensible tool for bio-imaging because of its advantages in terms of contrast, chemical specificity, three-dimensional sectioning capability, and so on. However, due to the quantum nature of light wave, the resolution for far-field optical imaging had long been limited to around half of the wavelength of the excitation light, which was found by Ernst Abbe in 1873 and is now well known as the diffraction limit. Recently, three-dimensional (3D) far-field optical imaging with a resolution beyond diffraction limit has attracted significant attention due to its potential for achieving electron microscope resolution in living cell imaging.[1] Several innovative techniques have been proposed, such as stimulated emission depletion microscopy (STED),[2] stochastic optical reconstruction microscopy (STORM),[3] photoactivatable localization microscopy (PALM),[4] saturated pattern excitation microscopy (SPEM),[5] 4Pi microscopies,[6,7] and so on. Generally speaking, super-resolution microscopes demonstrated so far are more complex and more expensive than a conventional scanning fluorescence

microscope in terms of focal geometry[5–7] and excitation light source.[2–4]

Recently, it has been found that super-resolution in 3D far-field imaging can be achieved with a conventional scanning fluorescence microscope based on linear fluorescence excitation, taking advantage of the saturation effect in the Förster resonant energy transfer (FRET) process between closely-spaced dye molecules.[8,9] The so-called saturated Förster resonant energy transfer microscopy (SFM), if combined with other super-resolution imaging techniques such as STED (termed FASTED in Ref. 9), will further allow for bringing down the imaging resolution to single molecular scale.

On the other hand, for 3D far-field imaging, another important issue is the unbalanced lateral and axial resolutions, as the focal spot created by a single objective lens always elongates along the axial direction.[10,11] To resolve this issue, it is recently found that simultaneous spatio-temporal focusing of a femtosecond laser pulse can provide isotropic resolution in all three dimensions by effectively reducing the confocal length.[12,13] Unfortunately, the temporal focusing technique is only applicable for fluorescence imaging based on multiphoton excitation, which requires use of longer wavelength and therefore usually results in degradation of optical resolution.[14,15] Another technique that is particularly effective for improving the axial resolution is the 4Pi microscopy, proposed by Hell *et al.*, in 1992.[10] However, one important drawback for 4Pi microscopy based on one-photon excitation is the strong sidelobes produced next to the main focal spot, which frequently results in artifacts. An elegant way to realize a nearly complete suppression of the sidelobes is to use two-color two-photon excitation in 4Pi microscope, as proposed by Chen *et al.*, which theoretically showed that an axial resolution of ∼78 nm can be achieved.[7] Nevertheless, the 4Pi 2C2P microscopy, which improves the axial resolution purely by increasing aperture angle of the focusing system, is essentially not an imaging technique that truly breaks the barrier of diffraction limit. In this contribution, we show that combination of the 4Pi microscopy and the SFM can provide significant advantages. First of all, the axial resolution can be greatly enhanced; secondly, the sidelobes in the focal spot produced by the 4Pi focusing system can be completely removed, giving rise to a clean background for bio-imaging applications.

2. Theoretical Background of 4Pi SFM

We have built a set of coupled rate equations for calculating the excitation probabilities for both donor and accepter dyes in silica nanobeads co-doped with Cy3 and Cy5 molecules (we assume that all the Cy3 and Cy5 molecules are closely spaced within a small area so that the FRET process between the Cy3 and Cy5 molecules occurs with a very high efficiency, e.g., ∼100%) in Ref. 8, which are given again below for readers' convenience:

$$\begin{cases} \dfrac{dn_D^E}{dt} = n_D^G I_E \sigma_E - n_D^E (k_D + k_F) \\ \dfrac{dn_A^E}{dt} = n_D^E k_F - n_A^E k_A \end{cases}, \quad \text{if } n_A^G \geq n_D^E, \tag{1a}$$

$$\begin{cases} \dfrac{dn_D^E}{dt} = n_D^G I_E \sigma_E - n_D^E k_D - n_A^G k_F \\ \dfrac{dn_A^E}{dt} = n_A^G k_F - n_A^E k_A \end{cases}, \quad \text{if } n_A^G \leq n_D^E, \tag{1b}$$

$$n_D^G + n_D^E = N_D, \tag{1c}$$

$$n_A^G + n_A^E = N_A, \tag{1d}$$

where $n_{D(A)}^E$ and $n_{D(A)}^G$ are the probabilities of the donor (acceptor) molecules at the excited and ground states, respectively. The excitation wavelength is carefully selected so as to excite only the donor molecules while the excitation of the acceptor molecules can be efficiently avoided, owing to the separated excitation spectral peaks of the donor and acceptor molecules. The laser intensity used for excitation of the donor is defined as I_E, and the excitation cross-section of the donor is defined as σ_E. In addition, $k_D = 1/\tau_D$, $k_A = 1/\tau_A$, and k_F are the rates of spontaneous emission from donor, acceptor, and the rate of energy transfer from donor to acceptor, respectively; and τ_D and τ_A are the spontaneous emission lifetimes of donor and acceptor molecules, respectively. It is noteworthy that in deriving Eqs. (1a)–(1d), we have assumed that the vibrational decay rates for both the donor and acceptor are much higher than k_D, k_A, and k_F. That is to say, the donors and acceptors are assumed to relax to the lowest vibrational energy levels of their excited states almost instantly after being excited.

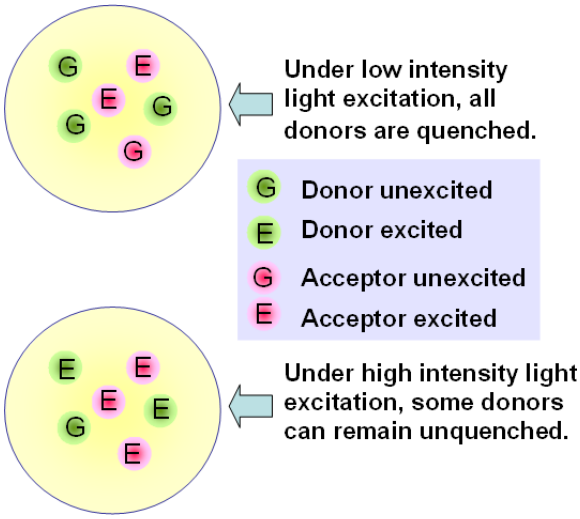

Fig. 1. Schematic of the energy transfer dynamics in silica nanobeads co-doped with Cy3 and Cy5 molecules experiencing donor excitation and FRET between donor and acceptor.

This condition is generally fulfilled for many dyes as the typical time scale of the vibrational decay is on the picosecond level, whereas the time scale of the spontaneous fluorescence emission is typically on the nanosecond level.

The physical picture corresponding to Eqs. (1) is illustrated in Fig. 1 and briefly explained as follows. At a low excitation intensity, the excited donor will be quenched by efficiently transferring its energy to the surrounding acceptors whenever there is unexcited acceptor molecules. However, at a high excitation intensity, the excited donor will be only partially quenched because of the limited spontaneous-emission-induced decay rate of the acceptors. The donors remaining at the excited state can then emit fluorescence light.

For continuous-wave (CW) excitation, the probability for the donor molecule staying at the excited state can be obtained as[8]

$$\begin{cases} n_D^E = N_D I_E \sigma_E / (I_E \sigma_E + k_D + k_F), \\ \quad \text{if } n_A^G = N_A - (k_F/k_A) n_D^E \geq n_D^E, \end{cases} \tag{2a}$$

$$\begin{cases} n_D^E = [N_D I_E \sigma_E - (N_A k_A k_F)/(k_A + k_F)]/ \\ \qquad (I_E \sigma_E + k_D), \\ \qquad \text{if } n_A^G = N_A k_A/(k_A + k_F) \leq n_D^E. \end{cases} \tag{2b}$$

Since the fluorescence intensity is proportional to n_D^E, we can calculate the optical resolution using Eq. (2).

3. Results

Our calculations are carried out using Eq. (2). Specifically, we assume that Cy3 and Cy5 dye molecules are used for constructing the silica nanobeads co-doped with donor and acceptor molecules, although in principle any FRET dyes that can ensure a high energy transfer efficiency (e.g., nearly ~100%) can be chosen for the SFM application. For the Cy3 and Cy5 molecules, we have $k_D \approx 3.3k_A$, which is determined by the fluorescence lifetimes of Cy3 (~0.3 ns) and Cy5 (~1 ns). Figure 2 illustrates the absorption and emission spectra of Cy3 and Cy5 molecules as well as the excitation wavelength and detection waveband chosen in our numerical simulation.

In Figs. 3(a) and 3(b), we compare the point-spread functions (PSFs) of a conventional confocal scanning fluorescence microscope equipped with an oil immersion objective of a numerical aperture (NA) of 1.40 (refractive index of oil: 1.51; semi-aperture angle: 67°) for two different kinds of fluorescent labels, namely, single Cy3 dye molecules and the silica nanobeads co-doped with Cy3 and Cy5 molecules, respectively. For both cases, we choose an excitation wavelength of 510 nm at which a high excitation efficiency of Cy3 molecules can be warranted whereas the excitation of Cy5 molecules can essentially be avoided (thus we can neglect the excitation of acceptor). Furthermore, the peak intensity at the center of the focal spot of the excitation beam is chosen to be $I_P = 3k_A/\sigma_E$. Under

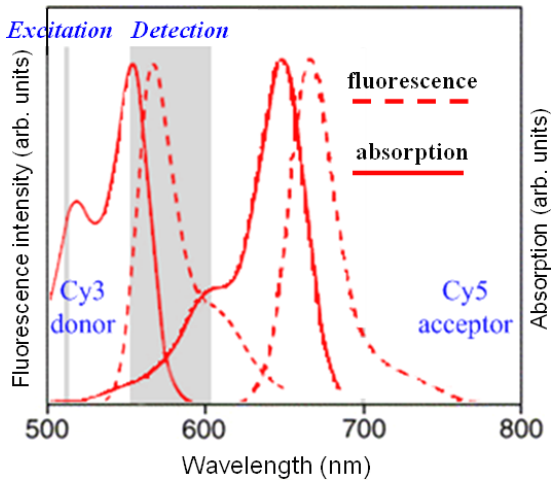

Fig. 2. Absorption and emission spectra of Cy3 and Cy5 dye molecules. Wavelengths of the excitation and detection light are also indicated.

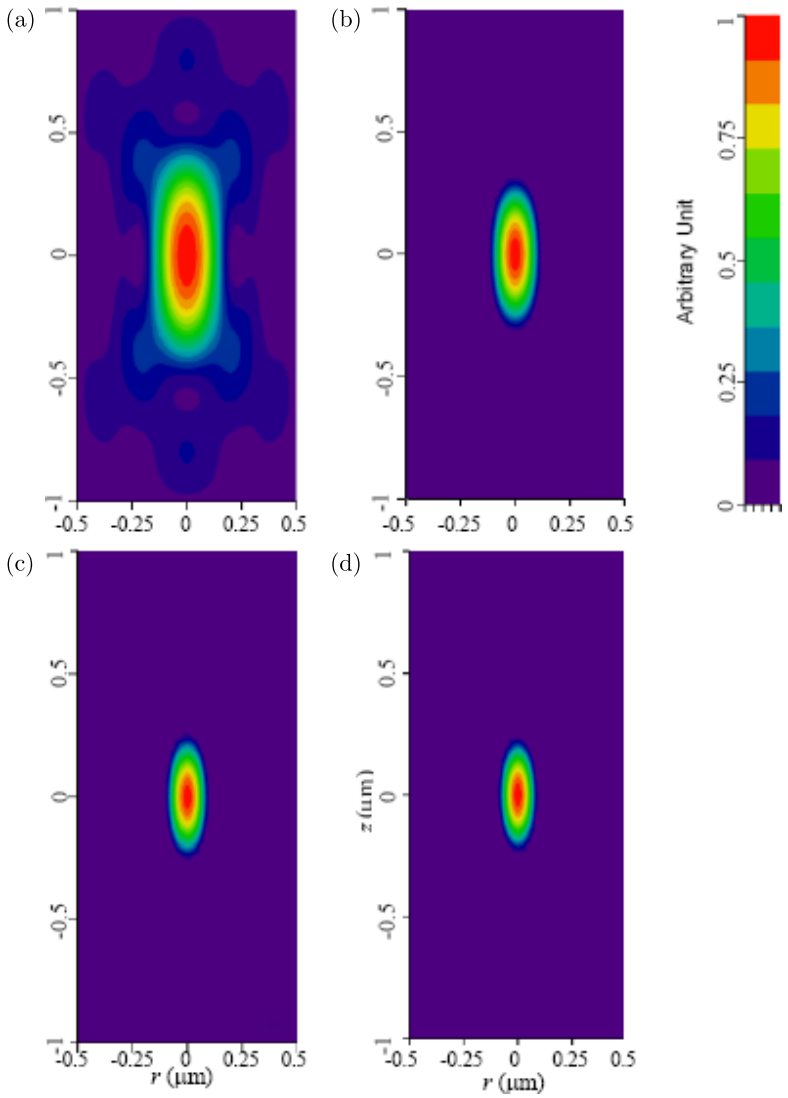

Fig. 3. Intensity distributions of fluorescence from Cy3 molecules excited by a CW beam at 510 nm when (a) single Cy3 dye molecules and (b)−(d) dye-co-doped nanobeads are used as fluorescent probes. Here, the results are obtained with a confocal microscope. The peak intensities at the center of the focal spot of the excitation beam are chosen to be (a), (b) $3k_A/\sigma_E$, (c) $2k_A/\sigma_E$, and (d) $1.8k_A/\sigma_E$. Color bar is given on the right-hand side in this figure.

these conditions, Fig. 3(a) shows the familiar PSF of the conventional scanning fluorescence microscope as one can expect; whereas in Fig. 3(b), the PSF of the same scanning fluorescence microscope, which uses the dye-co-doped silica nanobeads instead of the Cy3 molecules as fluorescence labels, is significantly size-reduced. The lateral and axial resolutions (full width at half-maximum, FWHM) for the PSF shown in Fig. 3(b) are calculated to be ∼163 and ∼438 nm, respectively. For comparison, the lateral and axial resolutions obtained at $I_P = 3k_A/\sigma_E$ for the conventional scanning fluorescence microscope are, respectively, ∼222 and ∼596 nm as shown in Fig. 3(a).

Shifting the peak excitation intensity close to (but still above) the threshold intensity $I_{\text{Threshold}} = k_A/\sigma_E$ leads to further improved spatial resolutions, as evidenced by the PSFs presented in Fig. 3(c). In Fig. 3(c), the peak excitation intensity is chosen to be $I_P = 2k_A/\sigma_E$, resulting in FWHM resolutions of ∼130 and ∼352 nm in the lateral and longitudinal directions, respectively. In Fig. 3(d), the peak excitation intensity is further reduced to $I_P = 1.8k_A/\sigma_E$, resulting in FWHM resolutions of ∼120 and ∼326 nm in the lateral and longitudinal directions, respectively. In all these cases, we clearly see that the axial resolutions are much worse than the lateral ones, which, as we will see below, can be improved by

employing the 4Pi focusing scheme. It is also noteworthy that although the peak excitation intensities for calculating the results in Figs. 3(c) and 3(d) are close, they will result in quite different results in terms of sidelobe intensity for the 4Pi-SFM microscopy [see Figs. 4(c) and 4(d)].

In Fig. 4, we compare the point-spread functions (PSFs) of 4Pi [Fig. 4(a)] and 4Pi-SFM [Figs. 4(b)–4(d)] microscopes equipped with a pair of oil immersion objective lenses with a numerical aperture (NA) of 1.40, same as that used in Fig. 3. All the other conditions, such as the excitation and detection wavelengths, as well as the dye labels, are the same as those used in Fig. 3. Also, the results in Figs. 4(b)–4(d) are obtained by assuming the excitation intensities to be $I_P = 3k_A/\sigma_E$, $I_P = 2k_A/\sigma_E$, $I_P = 1.8k_A/\sigma_E$, respectively. One can clearly see that in Fig. 4(b), the axial resolution is greatly improved. The axial FWHM width of the central lobe in Fig. 4(b) is only ~98 nm. However, it can also be seen that in Fig. 4(b), the sidelobes still remain strong. This is because of the relatively high excitation intensity at which the FRET process has already saturated at the central areas of the sidelobes. As we can see in Fig. 4(c), when the peak excitation intensity is reduced to $I_P = 2k_A/\sigma_E$, the sidelobes almost disappear. By further reducing the peak excitation intensity to $I_P = 1.8k_A/\sigma_E$,

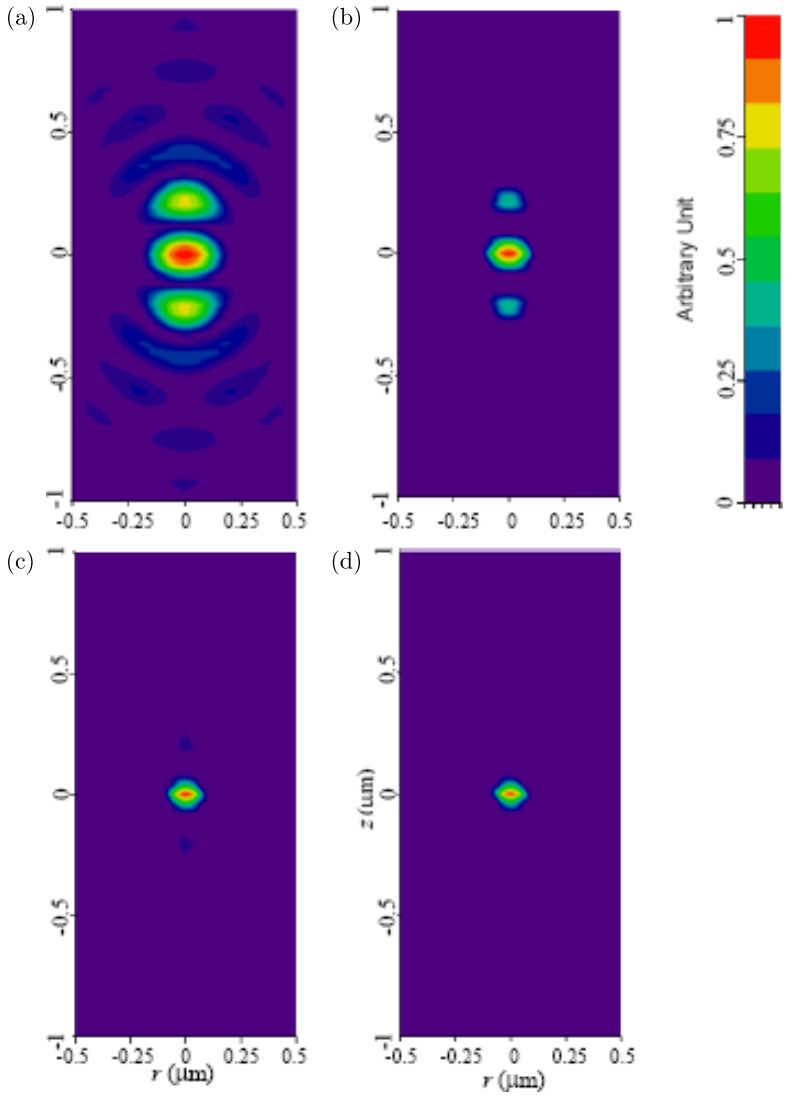

Fig. 4. Intensity distributions of fluorescence from Cy3 molecules excited by a CW beam at 510 nm when (a) single Cy3 dye molecules and (b)–(d) dye-co-doped nanobeads are used as fluorescent probes. Here, the results are obtained with a 4Pi microscope. The peak intensities at the center of the focal spot of the excitation beam are chosen to be (a), (b) $3k_A/\sigma_E$, (c) $2k_A/\sigma_E$, and (d) $1.8k_A/\sigma_E$. Color bar is given on the right-hand side in this figure.

the sidelobes can be completely suppressed in Fig. 4(d). Under this condition, the axial resolution can be improved to ∼73 nm, which is eight-fold enhanced as compared to that achievable with a conventional confocal microscope.

4. Conclusion

In conclusion, we have shown that the combination of 4Pi and SFM imaging techniques using dye-co-doped silica nanobeads can result in very high axial resolutions far beyond the diffraction limit, and consequently, lead to nearly isotropic resolution in all the three dimensions in space. In addition, since at a relatively low excitation intensity, the donor molecules can be effectively quenched via the FRET process, the sidelobes in the focal spot produced by the conventional 4Pi focusing system can be completely removed by carefully choosing the excitation intensity, leading to a clean background for bio-imaging using the single-photon 4Pi microscope.

Acknowledgment

J. Chen acknowledges the financial support from NSFC (Grant No. 61078016).

References

1. S. W. Hell, "Far-field optical nanoscopy," *Science* **316**, 1153−1158 (2007).
2. M. Dyba, S. W. Hell, "Focal spots of size $\lambda/23$ open up far-field fluorescence microscopy at 33 nm axial resolution," *Phys. Rev. Lett.* **88**, 163,901−163,904 (2002).
3. M. J. Rust, M. Bates, X. W. Zhuang, "Subdiffraction-limit imaging by stochastic optical reconstruction microscopy (STORM)," *Nat. Methods* **3**, 793−796 (2006).
4. E. Betzig, G. H. Patterson, R. Sougrat, O. W. Lindwasser, S. Olenych, J. S. Bonifacino, M. W. Davidson, J. Lippincott-Schwartz, H. F. Hess, "Imaging intracellular fluorescent *proteins at nanometer resolution*," *Science* **313**, 1642−1645 (2006).
5. M. G. L. Gustafsson, "Nonlinear structured-illumination microscopy: Wide-field fluorescence imaging with theoretically unlimited resolution," *Proc. Natl. Acad. Sci. USA* **102**, 13081−13086 (2005).
6. M. C. Lang, J. Engelhardt, S. W. Hell, "4Pi microscopy with linear fluorescence excitation," *Opt. Lett.* **32**, 259−261 (2007).
7. J. Chen, K. Midorikawa, "Two-color two-photon 4Pi fluorescence microscopy," *Opt. Lett.* **29**, 1354−1356 (2004).
8. J. Chen, Y. Cheng, "Far-field super-resolution imaging with dual-dye-doped nanoparticles," *Opt. Lett.* **34**, 1831−1833 (2009).
9. S. Deng, J. Chen, Q. Huang, C. Fan, Y. Cheng, "Saturated Förster resonance energy transfer microscopy with a stimulated emission depletion beam: A pathway toward single-molecule resolution in far-field bioimaging," *Opt. Lett.* **35**, 3862−3864 (2010).
10. S. W. Hell, E. H. K. Stelzer, "Fundamental improvement of resolution with a 4Pi-confocal fluorescence microscope using two-photon excitation," *Opt. Commun.* **93**, 277−282 (1992).
11. Y. Cheng, K. Sugioka, K. Midorikawa, M. Masuda, K. Toyoda, M. Kawachi, K. Shihoyama, "Control of the cross-sectional shape of a hollow microchannel embedded in photostructurable glass by use of a femtosecond laser," *Opt. Lett.* **28**, 55−57 (2003).
12. F. He, H. Xu, Y. Cheng, J. Ni, H. Xiong, Z. Xu, K. Sugioka, K. Midorikawa, "Fabrication of microfluidic channels with a circular cross section using spatiotemporally focused femtosecond laser pulses," *Opt. Lett.* **35**, 1106−1108 (2010).
13. F. He, Y. Cheng, J. Lin, J. Ni, Z. Xu, K. Sugioka, K. Midorikawa, "Independent control of aspect ratios in the axial and lateral cross sections of a focal spot for three-dimensional femtosecond laser micromachining," *New J. Phys.* **13**, 083014 (2011).
14. G. Zhu, J. V. Howe, M. Durst, W. Zipfel, C. Xu, "Simultaneous spatial and temporal focusing of femtosecond pulses," *Opt. Express* **13**, 2153−2159 (2005).
15. D. Oron, E. Tal, Y. Silberberg, "Scanningless depth-resolved microscopy," *Opt. Express* **13**, 1468−1476 (2005).